metals

MDPI

Article

Enhanced Ductility of a W-30Cu Composite by Improving Microstructure Homogeneity

Zehui Hao [1], Jinxu Liu [1,2,*], Jin Cao [1], Shukui Li [1,2,3], Xingwei Liu [1], Chuan He [1,2] and Xinying Xue [4]

1 School of Materials Science and Engineering, Beijing Institute of Technology, Beijing 100081, China; 2120161132@bit.edu.cn (Z.H.); 3120160524@bit.edu.cn (J.C.); bitleesk@bit.edu.cn (S.L.); 7520190032@bit.edu.cn (X.L.); chuan.he@bit.edu.cn (C.H.)
2 China National Key Laboratory of Science and Technology on Materials under Shock and Impact, Beijing Institute of Technology, Beijing 100081, China
3 State Key Laboratory of Explosion Science and Technology, Beijing Institute of Technology, Beijing 100081, China
4 Xi'an Modern Control Technology Research Institute, Xi'an 710065, China; xinying_xue@163.com
* Correspondence: liujinxu@bit.edu.cn; Tel.: +86-(010)-689-1393-7802

Received: 3 May 2019; Accepted: 31 May 2019; Published: 3 June 2019

Abstract: Due to its negligible solubility, it is difficult to obtain a W-30Cu composite with a homogenous microstructure. However, with a selected W skeleton, a homogeneous phase distribution was achieved for a W-30Cu composite in the present study. By detailed characterization of the mechanical performance and microstructure of the W-30Cu composite, as well as the stress distribution state under a loading condition, the effects of microstructure homogeneity on the mechanical properties and failure mechanisms are identified. The mechanisms by which the ductility and strength depend on microstructure homogeneity contain the effects on plastic deformation and stress coordination of the Cu phase network. The dominant factors for the high ductility and strength of W-30Cu composites are proposed.

Keywords: W-30Cu; microstructure homogeneity; dynamic compression strength; ductility; failure mechanism

1. Introduction

Tungsten–copper composites have been widely applied in electrical contact materials and heat sink materials due to their excellent properties of high electrical conductivity and good resistance to high temperature [1–3]. With the development of military technology, W-Cu composites have shown good potential in warhead materials that demand materials with good homogeneity and excellent dynamic mechanical properties (especially ductility) [4,5]. Particularly, W-30Cu composite shows an enormous potential in the military field due to its excellent comprehensive mechanical performance [6,7]. Compared with W-20Cu composite, the W-30Cu composite has a higher plastic deformation capacity and proper yield strength [8]. However, with the increase of copper content (particularly, from 20 wt.% to 30 wt.%), it would be more challenging to fabricate a W-Cu composite with a homogeneous microstructure via the conventional liquid phase sintering method due to the negligible solubility of the W-Cu system [9,10]. In general, to achieve homogenous distribution of the microstructure, the infiltration sintering method is commonly applied in the W-Cu system [11,12]. Ibrahim and Aziz [13] mentioned that subsequent infiltration treatment could increase the density and microstructure homogeneity of the W-Cu composite via liquid phase sintering. Further, to improve the sintering properties of the W-Cu composite, pre-treatments of powders such as mechanical

alloying [14,15], oxidation-reduction method [16], and preparation of Cu-coated W powders [17,18] have been investigated extensively.

It is known that W-W contiguity can be influenced significantly by Cu content and plays a dominant role in the mechanical performance of the W-Cu composite [19,20]. Since W-W contiguity will decrease according to the increase of Cu content, a considerable transformation of fracture behavior from brittle to ductile may occur in a W-Cu composite [21]. Furthermore, Deng et al. [22] fabricated a W-30Cu composite with a homogenous copper network structure by spark plasma sintering using core-shell powders. They confirmed that the W-Cu composite shows a homogeneous microstructure and high thermal conductivity due to the formation of a fine copper network structure and low W-W contiguity. However, detailed effects of microstructure homogeneity on mechanical properties for the W-30Cu composite are relatively deficient in previous studies.

In the present work, by inserting molten copper into the W-Cu skeleton and W skeletons, respectively, W-30Cu composites with different microstructure characteristics were fabricated. It is noteworthy that W powders with optimized particle sizes were used. Microstructure parameters were proposed to quantitatively describe the distribution features of the W and Cu phases. ANSYS LS-DYNA software was applied to simulate the stress distribution of the specimens during the deformation process, and high-speed photograph technology was used to record deformation behavior of specimens. The effects of microstructure homogeneity on mechanical properties and failure mechanisms under tensile and compressive tests were analyzed.

2. Materials and Methods

2.1. W-Cu and W Skeleton

For the first method, W and Cu powders with compositions of W-15 wt.% Cu were ball milled for 6 hours in a WC-Co container with WC-Co balls at a speed of 200 rpm. The weight ratio of ball to powders was 3:1. The milled powders were compacted at 250 MPa for 15 min by cold isostatic pressing to obtain a W-Cu skeleton. The W-30Cu compact was produced by infiltrating molten copper into the W-Cu skeleton. According to the processing steps (ball milling, compacting, and infiltrating (BCI)) the W-30Cu compact composite was named as the BCI composite. For the second method, to obtain a W skeleton with high porosity at a low compacting pressure, the particle size of W powders was first sifted and controlled within a narrow range. To obtain the W skeleton with proper porosity corresponding to the W-30Cu composite, the selected tungsten powders were compacted at various pressures and times by cold isostatic pressing without any pre-sintering treatment. Eventually, the tungsten powders were compacted at 100 MPa for 15 min to obtain a W skeleton. Another W-30Cu compact composite was produced by infiltrating molten copper into the W skeleton. According to the processing steps (sifting, compacting, and infiltrating (SCI)), the W-30Cu composite was named as the SCI composite. The isothermal infiltration processes of the W-Cu skeleton and W skeleton were performed for 2 h in dry H_2 at 1400 °C with a heating rate of 10 °C/min. Both desirable skeletons were infiltrated by oxygen-free molten copper.

The morphology and size distribution characteristics of two kinds of skeletons are given in Figure 1. It is seen that W particles possess a polyhedral morphology and a concentrated size distribution. The W-Cu skeleton is composed of copper and tungsten powders. Most of the copper particles with irregular shapes contain a broad particle size distribution and distribute around the tungsten powders. These large-sized copper particles can be converted into a copper pool after melting, which may promote the rearrangement of the tungsten particles, but the residual copper pool will cause copper phase aggregation after solidification. In a pure W skeleton, the W powder particles mainly exhibit a polygon shape with a diameter of 5–8 μm. The large-sized tungsten particles constitute the framework of the W skeleton, and the small-sized tungsten particles fill the gaps between the large particles. This is owing to the fact that fine tungsten particles are able to enter into the pores of the W skeleton by pressure applied during the compacting process [23]. The W particles can be rearranged randomly

by the capillary forces of molten copper, which are favorable to the homogenous microstructure of W-30Cu composite.

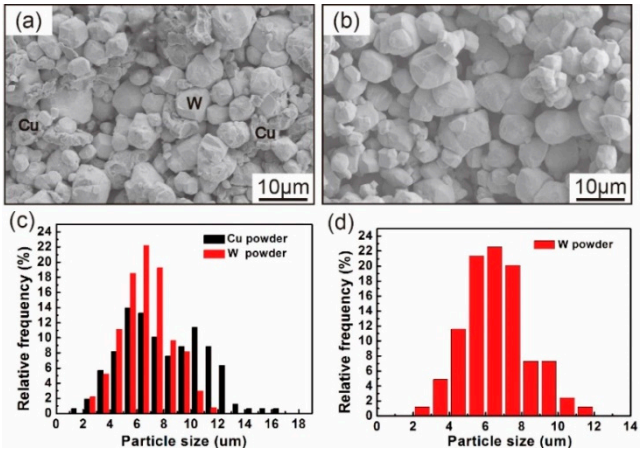

Figure 1. Microstructure morphology of skeletons: (**a**) W-Cu skeleton; (**b**) W skeleton. Size distribution characteristics of skeletons: (**c**) W-Cu skeleton; (**d**) W skeleton.

2.2. Experimental Method

The density of the W-30Cu composite was measured by the Archimedes method. The theoretical density was calculated by using inductively coupled plasma optical emission spectrometer (ICP-OES) method. Scanning electron microscopy (SEM) (Hitachi High–Technologies Corporation, Tokyo, Japan) and the Image-Pro Plus software (V6.0 For Windows, Media Cybernetics Corporation, Rockville, MD, USA) were employed to analyze the microstructure characteristics of the two kinds of composites. The SEM micrographs with different magnifications were applied to measure the W-W contiguity and phase distribution features.

The W-W contiguity $C_{W\text{-}W}$ was calculated using the following equation:

$$C_{W\text{-}W} = 2L_{W\text{-}W}/(2L_{W\text{-}W} + L_{W\text{-}Cu}) \quad (1)$$

where the $L_{W\text{-}Cu}$ and $L_{W\text{-}W}$ represent the length of the W/Cu and W/W interfaces respectively and were counted through the Image-Pro Plus software [24].

To quantitatively describe the distribution feature of W and Cu phase, a statistical parameter, i.e., the distribution homogeneity D_U, was proposed and calculated according to the following expression:

$$\frac{1}{D_U} = \sqrt{\frac{\sum_{i=1}^{n}\left(\frac{A_{Cu}}{A_W} - \overline{\frac{A_{Cu}}{A_W}}\right)^2}{n}} \quad (2)$$

where A_{Cu} and A_W represented the area of the Cu phase and W phase in SEM micrographs respectively, which are counted through the Image-Pro Plus software for each W-30Cu composite. n is the amount of statistical SEM micrographs. To make the statistic results more accurate, the value of n was at least greater than 10. The ratio of A_{Cu} to A_W was a constant if the phase distribution is completely homogenous, implying that the value of D_U tends to be infinite. Obviously, the larger the distribution homogeneity D_U, the more homogenous the distribution of the W and Cu phases is.

Quasi-static tensile tests under different temperature conditions were conducted. The tensile specimens were designed with dumbbell shapes, where the size of the reduced section was Φ5 mm × 25 mm. Quasi-static tensile tests were carried out using the CMT5150 universal testing machine with a strain rate of 10^{-3} s^{-1}. At least three specimens were prepared for tensile tests under different temperatures, respectively.

Furthermore, to clearly identify the effect of the microstructure homogeneity on the mechanical properties in the W-30Cu composite, a hollow specimen was designed for compressive tests. The geometry of the compressive specimen was designed as a hollow shaft of length L = 5 mm, with an outer diameter of 5 mm and inner diameter of 3 mm. Quasi-static compression tests were performed using CMT4150 universal testing machine with a strain rate of 10^{-3} s^{-1}, while the dynamic compression tests were carried out using split hopkinson pressure bar (SHPB) (Beijing Institute of Technology, Beijing, China) with a strain rate of 4500 s^{-1}. At least three specimens were tested for each condition. Furthermore, the deformation behavior of specimens under dynamic compression tests was captured via high-speed photograph technology. The Photron FASTCAM Mini AX200 high-speed camera (Photron, Tokyo, Japan) was used in the present work. In order to obtain more photos in the same time on the premise of adequate pixel resolution, 10,000 frames per second (fps) at 768 × 768 pixel resolution was chosen.

ANSYS LS-DYNA software (V15.0, Livermore Software Technology Corporation, Livermore, CA, USA) was utilized to simulate the stress distribution during the deformation process. The fracture surfaces of the specimens were observed by SEM to study the failure mechanism after compressive and tensile tests.

2.3. Simulation Model

According to the actual structure of the Split Hopkinson Pressure Bar device, the geometric models of the bullet, input bar, and output bar were established. The element type of bullet, input bar, and output bar are solid elements, while the element type of hollow specimens is a shell element. It is noted that the mapped mesh method is applied to reduce the calculating error in the mesh partition. The total number of elements reaches 325,136. To simplify the calculation of simulation, the bullet, input bar, and output bar were modeled through a rigid material model. The deformation process of compressive specimens was modeled through the material model "MAT_PIECEWISE_LINEAR_PLASTICITY". In this model, the stress–strain curve obtained from dynamic compression tests was selected for data fitting in our simulation. The tested material parameters used for the specimen simulation model are given in Table 1. Young's modulus and the material density of the W-30Cu composite applied in this simulation were obtained from the experimental results. Poisson's ratio is an empirical parameter. The initial condition of the simulation was set as follows: a bullet with a speed of 25 m/s strikes the input bar, corresponding to the bullet velocity in the actual experiment.

Table 1. Material parameters for specimen simulation model.

Quantity	Symbol	Value	Unit
Young's modulus	E	195	GPa
Poisson's ratio	M	0.35	-
Material density	ρ	14,330	Kg/m^3

3. Results and Discussion

3.1. Microstructure Characteristics

Quantitative characterizations of microstructure for W-30Cu composites are presented in Table 2. The distribution homogeneity D_U of the SCI composite is 9.09 which is much higher than that of the BCI (0.7). Further, the contiguity $C_{W\text{-}W}$ of the SCI composite is 0.38. However, the $C_{W\text{-}W}$ of BCI is 0.49. The results imply that, compared with BCI composite, the phase distribution is more homogeneous in the SCI composite. A tungsten skeleton in the form of "isolated island" morphology distributes homogeneously in the continuous copper network. In the SCI composite, polyhedral W grains have a homogeneous distribution feature in the Cu matrix, which possesses a continuous network structure, as shown in Figure 2a. By contrast, W grains with aggregated distribution exist in the Cu matrix in the BCI composite, as shown in Figure 2b, which is attributed to the large-sized copper powders in the

initial W-Cu skeleton. The copper network shows a phenomenon of "interruptions", where tungsten particles aggregate together.

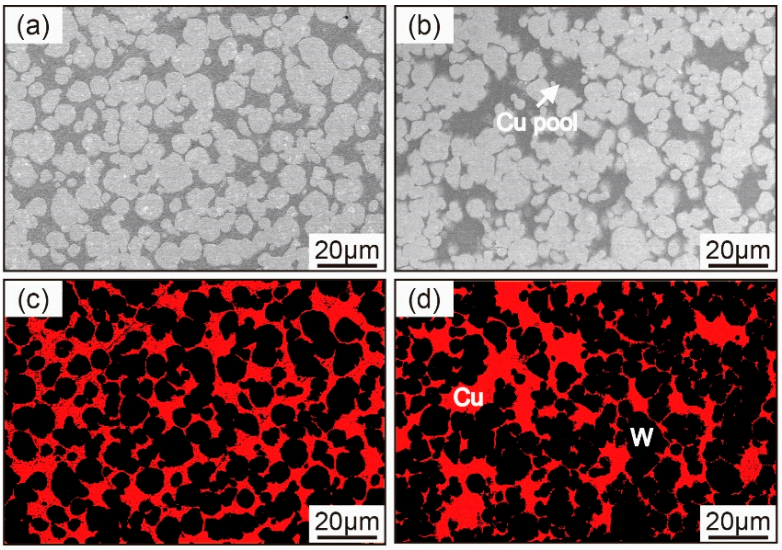

Figure 2. Microstructure of W-30Cu composites prepared by different process: (**a**) and (**c**) microstructure of the sifting, compacting, and infiltrating (SCI) composite; (**b**) and (**d**) microstructure of the ball milling, compacting, and infiltrating (BCI) composite.

Table 2. Microstructure parameters of W-30Cu composites.

Quantity	SCI Composite	BCI Composite
Relative density	98.5%	97.6%
Distribution homogeneity D_U	9.09	0.70
W-W contiguity $C_{W\text{-}W}$	0.38	0.49

3.2. Tensile Test

The true stress–strain curves under tensile conditions for the W-30Cu composites as a function of temperature are plotted in Figure 3a,b. It can be seen that temperature plays an important role in the tensile mechanical properties. The tensile properties of the W-30Cu composites exhibit remarkable temperature dependence and follow the same trend: with an increase of testing temperature, the strength value reaches its maximum at room temperature and then decreases, while the percent elongation reaches its maximum at 300 °C and then sharply decreases. As depicted in Figure 3c in detail, the strength of the SCI composite is higher than that of the BCI composite within a given temperature range from 25 °C to 600 °C. In Figure 3d, the tensile percent elongation as a function of temperature is given for the W-30Cu composites. It is noted that the SCI composite exhibits a higher value in tensile elongation within the given testing temperature range. At room temperature, tensile elongation of the SCI composite is 10.2%, while the tensile elongation of the BCI composite is only 6.51%. Considering the microstructure characteristics of W-30Cu composites, these results indicate that a homogeneous microstructure can lead to a significant advantage in tensile mechanical performance.

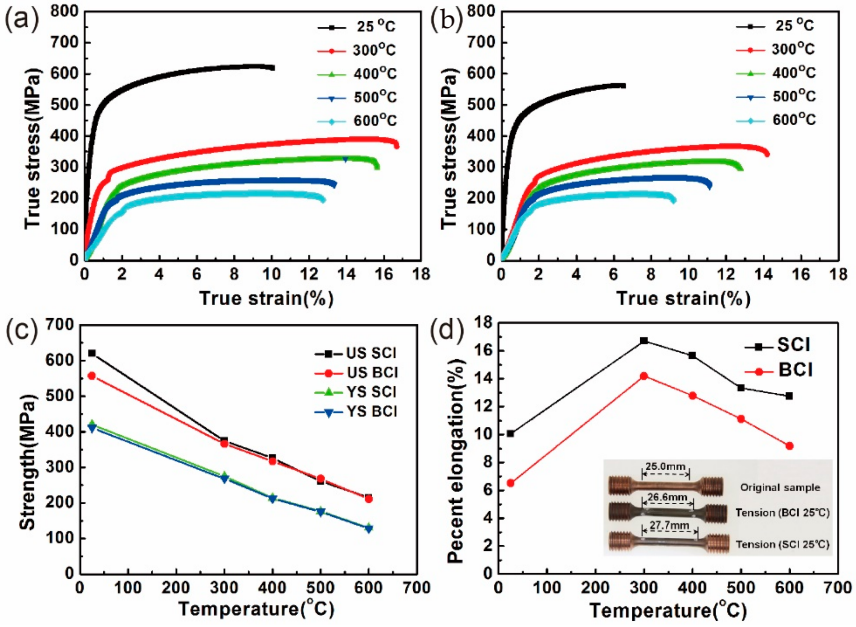

Figure 3. Quasi-static tensile tests of W-30Cu composites: (**a**) true stress–strain curve of the SCI composite; (**b**) true stress–strain curve of the BCI composite; (**c**) tensile strength-temperature curve; (**d**) percent elongation–temperature curve.

Figure 4 presents the typical fracture surfaces of the W-30Cu composites after tensile testing at 25 °C, 300 °C and 500 °C. At room temperature, as shown in Figure 4a,b, the deformation of the Cu phase with the typical dimples and intergranular fractures of W particles dominate the failure of the W-30Cu composites. However, the cleavage that occurred in the W-W interfaces can be observed as a result of the presence of W phase agglomeration, as shown in Figure 4b, while the W phase is surrounded by continuous well-deformed copper in Figure 4a. The deformation of the copper phase in the SCI composite is more prominent and particularly visible. Furthermore, with an increase of the testing temperature, an appreciable number of micro-cracks appear on the fracture surface in the BCI composite (Figure 4d). The fracture surface shows uneven morphology, with a valley in the depth (Figure 4f). It is noticeable that either visible micro-cracks or uneven surface provide direct evidence for the inhomogeneous deformation of the BCI composite at room temperature, as well as high temperatures. The deformation degree of the Cu phase represents a crucial factor affecting the tensile ductility of the W-30Cu composite. As a consequence, the SCI composite with superior tensile ductile performance can be attributed to its continuous copper network and homogenous phase distribution features. Although the difference in microstructure homogeneity can lead to a difference in ductility, the two kinds of composites exhibit similar temperature dependence. As shown in Figure 4c,d, as a result of the dimples fraction increasing and reaching the maximum at 300 °C, the fracture surfaces shows transition phenomena from a rough surface at room temperature to a smooth surface at 300 °C. As we know that copper displays features of "intermediate temperature embrittlement" [25], the ductility of the Cu phase may have been weakened as the testing temperature increased above 400 °C, which may have led to stress concentrations at W/Cu interfaces, thus destroying the W/Cu interfaces, as shown in Figure 4e,f. In previous studies [26,27], the Cu phase can cause local crack deflection and generate an extensive plastic deformation at low temperatures (T < 400 °C). However, the degradation in ductility of the Cu phase is the main reason for early failure of W-Cu composites at high temperatures (T > 400 °C).

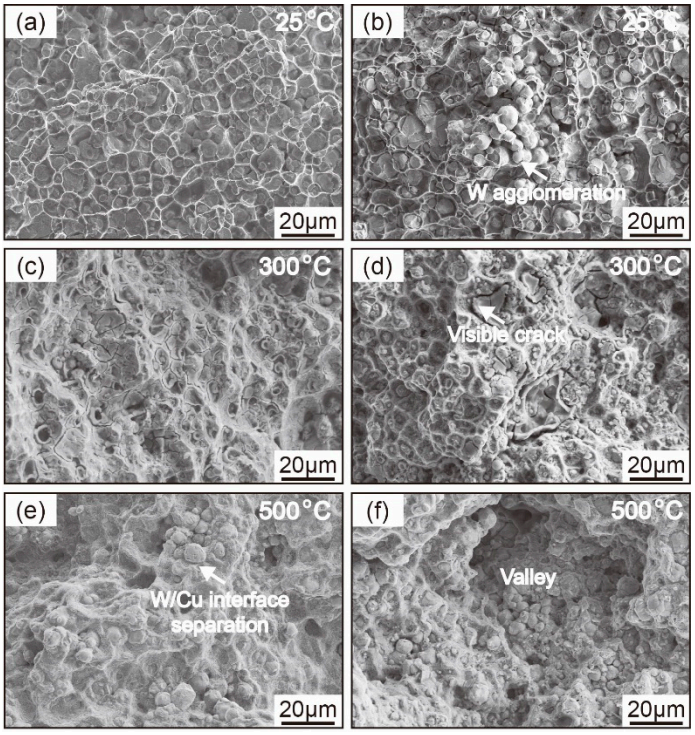

Figure 4. SEM micrographs of the fracture surfaces of W-30Cu composites after tensile testing at different temperatures: (**a**) SCI composite at 25 °C; (**b**) BCI composite at 25 °C; (**c**) SCI composite at 300 °C; (**d**) BCI composite at 300 °C; (**e**) SCI composite at 500 °C; (**f**) BCI composite at 500 °C.

3.3. Compression Test

To study the stress distribution and deformation behavior of the two kinds of composites, a hollow cylindrical specimen was designed for compression tests in this work. The true stress–strain curve of W-30Cu composites under dynamic compression conditions is plotted in Figure 5a. It can be found that the SCI composite exhibits a higher failure strain of 23.6%. In contrast, the failure strain of the BCI composite is 13.9%. Furthermore, the strength of the SCI composite exhibits a constant stage, while the strength of the BCI composite reaches its maximum at a strain of 12% and then drops off rapidly. The different mechanical behaviors of the two composites indicate that a homogeneous microstructure can contribute to homogenous plastic deformation under dynamic compression conditions.

To visually describe the stress distribution under dynamic compression conditions, stress nephograms at different simulation moments were obtained via ANSYS LS-DYNA software (V15.0, Livermore Software Technology Corporation, Livermore, CA, USA). In Figure 5b, it can be found that the stress exhibits the same level in the whole specimen when the simulation time reaches 0.14 ms. The value of stress is mainly in the order of 970MPa. As shown in Figure 5c, the stress gradually increases with the increase of simulation time. Particularly, the maximum value of stress is observed around the center of the inner surface before failure. Thus, for hollow specimens, stress waves rapidly pass and reflect through the whole specimen due to its thin-wall structure. The stress reaches a high value in a short time and the stress distribution is relatively homogeneous, which demands that the W-Cu composites should contain high strength and deformation capabilities.

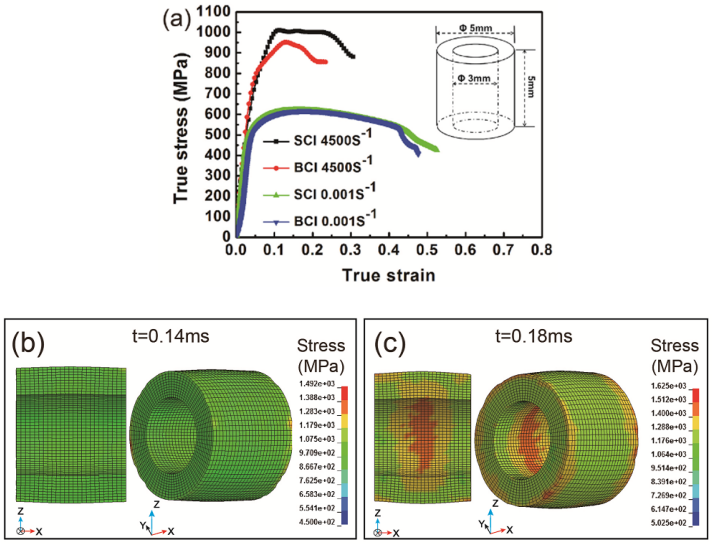

Figure 5. Mechanical performance and finite element modelling under compressive tests for W-30Cu composites at room temperature: (**a**) true stress–strain curve; (**b**) stress distribution at 0.14 ms; (**c**) stress distribution at 0.18 ms.

For a better representation of evolution in material failure, as shown in Figure 6, the deformation behaviors of the W-30Cu composites are captured by using high-speed photograph technology. Under dynamic compression conditions, the SCI composite presents obvious plastic deformation in Figure 6a. By contrast, in Figure 6b, the BCI composite shows rigid characteristics, which correspond to the sharp decrease of stress values in Figure 5a. Furthermore, a significant amount of tiny debris can be found in the SCI composite under dynamic compression, as shown in Figure 6c, while several fragments appear in the BCI composite in Figure 6d. These results indicate that, for the SCI composite, homogeneous phase distribution can facilitate continuous plastic deformation and high dynamic compressive strength.

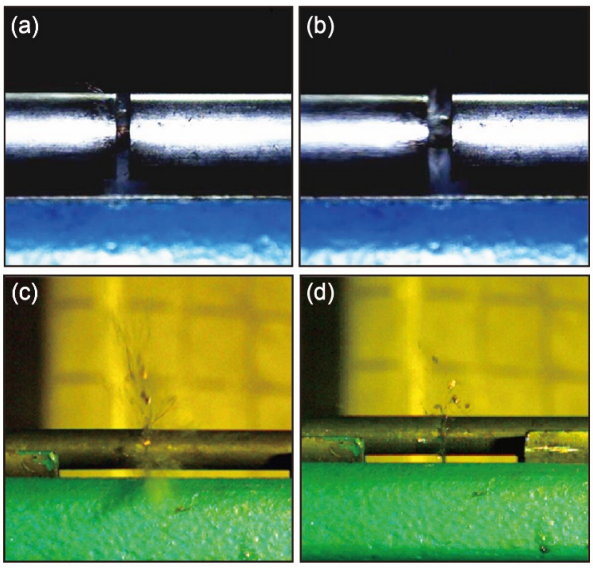

Figure 6. High speed photographs of W-30Cu composites under dynamic compression conditions: (**a**) the SCI composite with plastic deformation; (**b**) the BCI composite without plastic deformation; (**c**) the destructed SCI composite with tiny debris; (**d**) the destructed BCI composite with several fragments.

To study the failure mechanism of the W-30Cu composites, the fracture surfaces after dynamic compression testing are investigated as shown in Figure 7. For the SCI composite, as shown in Figure 7a, the deformation of the Cu phase is obvious and continuous. Moreover, the micro-cracks are generated at the interface of the W/W or W/Cu and are isolated in the well-deformed Cu phase. In contrast, for the BCI composite, the micro-cracks propagate along the interface of the W/W at the location of the W-phase agglomeration. Indeed, the Cu matrix plays a significant role in the plastic deformation and coordination of stress concentration. Simultaneously, the W particles show slight elongation in the W-Cu composites under dynamitic compression conditions [28].

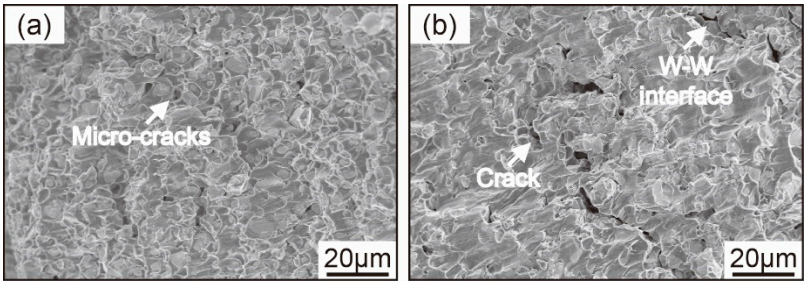

Figure 7. SEM micrographs of the fracture surfaces of W-30Cu composites under dynamic compression conditions: (**a**) the SCI composite; (**b**) the BCI composite.

Combining the results on the deformation behaviors and fracture surface morphology of W-30Cu composites under dynamic compression conditions, the relationship between microstructure homogeneity and compressive mechanical performance is established. Under the dynamic compression conditions of the hollow specimens, the stress with a high value distributes homogeneously within the whole specimen. In general, interfaces of W/W or W/Cu are readily propagated by micro-cracks due to their poor bonding strength. As for the SCI composite, due to its homogenous Cu phase distribution, micro-cracks nucleate and propagate randomly. Furthermore, it is known that the nucleation and propagation of micro-cracks are mainly prohibited and compensated by the coordinated deformation of a Cu phase network. The number of micro-cracks increases throughout the whole specimen until the rupture of the Cu phase dominates the fracture mechanism of the W-Cu composite, finally leading to the failure of the W-30Cu composite as a result of producing significant amounts of tiny debris. On the contrary, in the BCI composite, the micro-cracks nucleate intensively at the location of the W phase agglomeration. Due to the inhomogeneous distribution of the copper phase, the micro-cracks cannot be prohibited timely by the copper phase, leading micro-cracks to coalesce and then propagate along the W-W interface. Consequently, the BCI composite specimen breaks into several fragments. These results indicate that the excellent advantage of the SCI composite in ductility is caused by its homogeneous phase distribution and continuous Cu phase network.

4. Conclusions

In the present study, by infiltrating molten Cu phase into W skeleton and W-Cu skeleton, W-Cu composites with different homogeneity of phase distribution were prepared. The effects of microstructure homogeneity on the mechanical properties and failure mechanisms under tensile and compressive conditions were investigated. The relationship between microstructure characteristics and the failure of W-30Cu composites was studied in detail. The related conclusions are mentioned below:

1. The selected tungsten powders were compacted by isostatic cool pressing at 100 MPa to obtain a W skeleton. The W-30Cu composite was prepared via infiltrating molten copper into the W skeleton. The prepared W-30Cu composite exhibits homogeneous phase distribution feature and continuous Cu phase network structure.
2. Quasi-static tensile tests of W-30Cu composites with a different homogeneity of phase distribution were investigated. It was found that tensile elongation of the SCI composite is 10.2% while the

BCI composite is only 6.51% at room temperature. It was confirmed that the homogeneous phase distribution feature and continuous network structure are responsible for a high capacity of plastic deformation in the W-30Cu composites. Further, as a function of temperature, both the SCI and BCI composite display a similar ductile evolution with an increase in temperature. In addition, their tensile elongation reaches a maximum of 16.7% and 14.1% for the SCI composite and the BCI composites, respectively, at 300 °C.

3. Hollow cylindrical specimens were applied to study the effect of microstructure homogeneity on strength and ductility of the W-30Cu composites under a dynamic compression condition. The SCI composite exhibits an excellent plastic deformation capacity due to its homogenous distribution feature and continuous network structure. The micro-cracks nucleate randomly instead of concentrating on the location of the W phase agglomeration due to the homogeneous phase distribution feature, and the micro-cracks can be prohibited and compensated by the coordinated deformation of the continuous copper network.

Author Contributions: Conceptualization, methodology, and formal analysis, Z.H. and J.L.; investigation and software, Z.H. and J.C.; writing—original draft preparation, Z.H.; writing—review and editing, Z.H., X.L. and C.H.; resources and funding acquisition, S.L. and X.X.

Funding: This research is supported by the funding of the National Key R&D Program of China (2017YFB0306000) and The National Science Foundation of China (No. 51571033). This work was supported in part by the National Natural Science Foundation of China under Grant (No. 11521062).

Acknowledgments: The China National Key Laboratory of Science and Technology on Materials under Shock and Impact is acknowledged.

Conflicts of Interest: The authors declare no conflict of interest.

References

1. Li, J.; Deng, N.; Wu, P.; Zhou, Z. Elaborating the Cu-network structured of the W–Cu composites by sintering intermittently electroplated core-shell powders. *J. Alloys Compd.* **2019**, *770*, 405–410. [CrossRef]
2. Meng, Y.; Shen, Y.; Chen, C.; Li, Y.; Feng, X. Effects of Cu content and mechanical alloying parameters on the preparation of W–Cu composite coatings on copper substrate. *J. Alloys Compd.* **2014**, *585*, 368–375. [CrossRef]
3. Muller, A.; Ewert, D.; Galatanu, A.; Milwich, M.; Neu, R.; Pastor, J.Y.; Siefken, U.; Tejado, E.; You, J.H. Melt infiltrated tungsten–copper composites as advanced heat sink materials for plasma facing composites of future nuclear fusion devices. *Fusion Eng. Des.* **2017**, *124*, 455–459. [CrossRef]
4. Wang, F.; Guo, W.; Liu, J.; Li, S.; Zhou, J. Microstructural evolution and grain refinement mechanism of pure tungsten under explosive loading condition. *Int. J. Refract. Met. Hard Mater.* **2014**, *45*, 64–70. [CrossRef]
5. Elshenawy, T.; Elbeih, A.; Li, Q.M. A modified penetration model for copper-tungsten shaped charge jet with non-uniform density distribution. *Cent. Eur. J. Energetic Mater.* **2016**, *13*, 927–943. [CrossRef]
6. Wang, F.; Jiang, J.; Men, J.; Bai, Y.; Wang, S.; Li, M. Investigation on shaped charge jet density gradient for metal matrix composites: Experimental design and execution. *Int. J. Impact Eng.* **2017**, *109*, 311–320. [CrossRef]
7. Xi, B.; Liu, J.; Li, S.; Lv, C.; Guo, W.; Wu, T. Effect of interaction mechanism between jet and target on penetration performance of shaped charge liner. *Mater. Sci. Eng. A* **2012**, *553*, 142–148. [CrossRef]
8. Guo, W.; Wang, Y.; Liu, K.; Li, S.; Zhang, H. Effect of Copper Content on the Dynamic Compressive Properties of Fine-grained Tungsten Copper Alloys. *Mater. Sci. Eng. A* **2018**, *727*, 140–147. [CrossRef]
9. Johnson, J.L.; Brezovsky, J.J.; German, R.M. Effect of liquid content on distortion and rearrangement densification of liquid-phase-sintered W-Cu. *Metall. Mater. Trans. A* **2005**, *36*, 1557–1565. [CrossRef]
10. Elsayed, A.; Li, W.; Kady, O.A.E.; Daoush, W.M.; Olevsky, E.A.; German, R.M. Experimental investigations on the synthesis of W–Cu nanocomposite through spark plasma sintering. *J. Alloys Compd.* **2015**, *639*, 373–380. [CrossRef]
11. Hamidi, A.; Arabi, H.; Rastegari, S. Tungsten-copper composite production by activated sintering and infiltration. *Int. J. Refract. Met. Hard Mater.* **2011**, *29*, 538–541. [CrossRef]

12. Ahangarkani, M.; Zangeneh-Madar, K.; Borji, S. Microstructural study on the effect of directional infiltration and Ni activator on tensile strength and conductivity of W-10wt%Cu composite. *Int. J. Refract. Met. Hard Mater.* **2018**, *71*, 340–351. [CrossRef]
13. Ibrahim, H.; Aziz, A.; Rahmat, A. Enhanced liquid-phase sintering of W–Cu composites by liquid infiltration. *Int. J. Refract. Met. Hard Mater.* **2014**, *43*, 222–226. [CrossRef]
14. Li, C.; Zhou, Y.; Xie, Y.; Zhou, D.; Zhang, D. Effects of milling time and sintering temperature on structural evolution, densification behavior and properties of a W-20wt.%Cu alloy. *J. Alloys Compd.* **2018**, *731*, 537–545. [CrossRef]
15. Qiu, W.T.; Pang, Y.; Xiao, Z.; Li, Z. Preparation of W-Cu alloy with high density and ultrafine grains by mechanical alloying and high pressure sintering. *Int. J. Refract. Met. Hard Mater.* **2016**, *61*, 91–97. [CrossRef]
16. Wang, C.P.; Lin, L.C.; Xu, L.S.; Xu, W.W.; Song, J.P.; Liu, X.J.; Yu, Y. Effect of blue tungsten oxide on skeleton sintering and infiltration of W–Cu composites. *Int. J. Refract. Met. Hard Mater.* **2013**, *41*, 236–240. [CrossRef]
17. Zhou, Q.; Chen, P. Fabrication of W–Cu composite by shock consolidation of Cu-coated W powders. *J. Alloys Compd.* **2016**, *657*, 215–223. [CrossRef]
18. Zhang, Q.; Liang, S.; Zhuo, L. Fabrication and properties of the W-30wt%Cu gradient composite with W@WC core-shell structure. *J. Alloys Compd.* **2017**, *708*, 796–803. [CrossRef]
19. Hiraoka, Y.; Inoue, T.; Hanado, H.; Akiyoshi, N. Ductile-to-Brittle Transition Characteristics in W–Cu Composites with Increase of Cu Content. *Mater. Trans.* **2005**, *46*, 1663–1670. [CrossRef]
20. Ahangarkani, M.; Borji, S.; Zangeneh-madar, K.; Valefi, Z.; Ahangarcani, M. Mutual relationship between material removal rate and W-W interfacial features during ultra-high temperature erosion of infiltrated W-10wt.%Cu composite. *Int. J. Refract. Met. Hard Mater.* **2018**, *75*, 191–201. [CrossRef]
21. Tejado, E.; Muller, A.V.; You, J.-H.; Pastor, J.Y. The thermo-mechanical behaviour of W-Cu metal matrix composites for fusion heat sink applications: The influence of the Cu content. *J. Nucl. Mater.* **2018**, *498*, 468–475. [CrossRef]
22. Deng, N.; Zhou, Z.; Li, J.; Wu, Y. W-Cu composites with homogenous Cu-network structure prepared by spark plasma sintering using core-shell powders. *Int. J. Refract. Met. Hard Mater.* **2019**, *82*, 310–316. [CrossRef]
23. Montealegre-Meléndez, I.; Arévalo, C.; Perez-Soriano, E.W.; Neubauer, E.; Rubio-Escudero, C.; Kitzmantel, M. Analysis of the Influence of Starting Materials and Processing Conditions on the Properties of W/Cu Alloys. *Materials* **2017**, *10*, 142. [CrossRef] [PubMed]
24. Zheng, L.; Liu, J.; Li, S.; Wang, G.; Guo, W. Investigation on preparation and mechanical properties of W–Cu–Zn alloy with low W–W contiguity and high ductility. *Mater. Des.* **2015**, *86*, 297–304. [CrossRef]
25. Laporte, V.; Mortensen, A. Intermediate temperature embrittlement of copper alloys. *Int. Mater. Rev.* **2009**, *54*, 94–116. [CrossRef]
26. Tejado, E.; Muller, A.V.; You, J.-H.; Pastor, J.Y. Evolution of mechanical performance with temperature of W/Cu and W/CuCrZr composites for fusion heat sink applications. *Mater. Sci. Eng. A* **2018**, *712*, 738–746. [CrossRef]
27. Zivelonghi, A.; You, J.-H. Mechanism of plastic damage and fracture of a particulate tungsten-reinforced copper composite: A microstructure-based finite element study. *Comput. Mater. Sci.* **2014**, *84*, 318–326. [CrossRef]
28. Guo, W.; Liu, J.; Li, S.; Wang, Y.; Ji, W. Microstructural evolution and deformation mechanism of the 80W-20Cu alloy at ultra-high strain rates under explosive loading. *Mater. Sci. Eng. A* **2013**, *572*, 36–44.

© 2019 by the authors. Licensee MDPI, Basel, Switzerland. This article is an open access article distributed under the terms and conditions of the Creative Commons Attribution (CC BY) license (http://creativecommons.org/licenses/by/4.0/).